15th IFK
Proc. of the 15th International Fluid Power Conference <Symposium/Conference>
<DOI>

Effects of contamination on the wear process of piston/cylinder interface in axial piston machines considering three-body abrasive wear model

Liangyu Song[1], Fei Lyu[1,2]*, Junhui Zhang [1], Bing Xu [1]

[1] *The State Key Laboratory of Fluid Power and Mechatronic Systems, Zhejiang University, 866 Yuhangtang Road, Hangzhou, Zhejiang 310058, China*

[2] *Institute for Fluid Power Drives and Systems, RWTH Aachen University. Campus-Boulevard 30, 52074 Aachen, Germany*

* *Corresponding author: Tel.: (49)1739447126; E-mail address: fei.lyu@ifas.rwth-aachen.de*

Abstract.

Contamination level is a critical indicator in hydraulic systems. The piston/cylinder interface (PCI) serves vital functions in lubrication and load-bearing within axial piston pumps. Under contaminated conditions, PCI performance degrades rapidly, potentially resulting in complete pump failure. A wear model incorporating multiple wear mechanisms at the PCI was developed, along with a predictive method specifically accounting for three-body abrasive wear. An isolated PCI test bench that can accurately control the contamination degree was designed for verification. Both simulation and experimental results demonstrate that contaminated abrasive particles alter wear distribution and significantly accelerate the wear process.

Keywords. Contamination level, piston/cylinder interface, three-body abrasive wear, abrasive particle, wear process prediction.

1. INTRODUCTION

Axial piston machines are widely used as hydraulic power sources in industrial operation systems, offering higher power density in high-pressure applications. The piston/cylinder interface (PCI) is a critical tribological interface in axial piston machines, responsible for lubrication and load support. During operation, this interface undergoes increased wear caused by various mechanisms, including adhesive wear, two-body abrasive wear, and three-body abrasive wear induced by the rolling action of entrained wear particles within the contact interface. These complex wear mechanisms can degrade the oil suction and discharge performance and eventually lead to system failure.

Analyzing the wear process of the piston-cylinder interface (PCI) is crucial for effective predictive maintenance, accurately assessing its service life and reliability, and providing key insights for design optimization aimed at wear resistance and anti-wear properties. During operation, the surface contour of the piston/cylinder pair degenerates over time, accompanied by complex oil film pressure and thickness boundaries. As a result, the wear state of the interface is highly dynamic and coupled with oil film characteristics. Fei Lyu et al. conducted numerical simulations on two-body abrasive and adhesive wear processes of the piston-cylinder interface (PCI) [1,2]. Yu Lin et al. established a dynamic model based on the equivalent load method and proposed a novel wear prediction approach for the PCI by integrating the Archard wear model [3]. Lars Brinkschulte et al. proposed a simulation model, based on the Archard and Fleischer approaches, to predict wear in the piston-cylinder contact [4]. Roman Ivantysyn et al. combined numerical simulation with experimental measurements to analyze the run-in wear behavior of the slipper-swash plate interface in axial piston pumps, demonstrating the stabilization of the lubricating gap and wear profile during early operation [5]. Zunling Du et al. established a mixed lubrication model for the slipper pair within an elasto-hydrodynamic lubrication (EHL) framework, integrating two-body abrasive and Archard adhesive wear theories to formulate an eccentric wear prediction method [6]. Svenja Horn et al. investigated the tribological performance of different slipper designs in axial piston pumps, showing that tailored surface structures can effectively enhance hydrodynamic pressure generation and improve wear condition under mixed lubrication conditions [7]. Xuguang Li et al. proposed a wear prediction model for the cylinder block/valve plate interface, considering the multi-scale evolution of surface topography, including both macroscopic profile wear and microscopic asperity deformation [8].

However, the impact of high oil contamination levels was not considered in these simulations. High contamination levels can cause severe wear on the friction pairs, especially under high-pressure and high-speed PCI conditions, which are more sensitive to contamination levels [9]. Compared with other friction pairs such as the slipper-swash plate interface and the cylinder block/valve plate interface, the PCI shows a stronger dependence of its frictional behavior on clearance design, resulting in increased sensitivity to contaminant particles [10]. The distribution of abrasive particle size and concentration is related to the level of contamination, such as the standard NAS1638 for oil contamination level [11]. Three-body abrasive wear, which is caused by abrasive particles entering the friction pairs, is significantly influenced by the size, hardness, and concentration of the abrasive particles. Therefore, studying three-body abrasive wear of PCI under high contamination levels is crucial for better predicting the wear process.

There is extensive basic research on three-body wear of tribo-pairs. Under high oil pollution conditions, three-body abrasive wear accounts for a large proportion [12], which affects the service life and performance of friction pairs. Different types and sizes of contaminant particles in oil can lead to different wear results of friction pairs [13]. Some studies have explored the effects of materials, textured surfaces, and abrasive particle sizes on the wear process of bearings [14,15]. Nejc Novak et al. studied the effect of oil contaminants on accelerated gear wear [16]. The performance of lubricants and coatings can also affect three-body abrasive wear [17,18]. However, the extreme operating conditions of PCI lead to complex boundary conditions that form wedge-shaped oil films and multiple wear mechanisms acting simultaneously. These studies mainly analyze local specific wear through wear experiments, and there is no way to directly analyze the distributed lubrication state and multiple complex wear mechanisms in PCI. Therefore, it is necessary to study the coupling of wear and oil film in PCI after considering three-body wear.

This paper proposes a method for predicting wear process in the PCI that incorporates three-body abrasive wear caused by contaminated oil. Section 2 outlines the simulation of lubrication calculation and wear cycle. Section 3 describes the experimental setup for testing a single PCI under different contamination conditions. Section 4 compares simulated and experimental results. Section V concludes the study.

2. WEAR PROCESS SIMULATION

The development of a PCI wear model begins with a dynamic analysis to calculate lubrication boundary conditions such as oil film pressure and thickness. Following this, a distributed wear sub-model performs the wear calculation. The resulting updated contour is then coupled with the oil film, enabling the prediction of the wear process.

2.1. Dynamic Analysis and Lubrication Calculation of PCI

Figure 2.1 shows the general configuration of the axial piston pump, the main external forces applied on the piston are shown in Figure 2.2. The support force of the swash plate F_{SS} and the pressure force F_{P} cause the piston to reciprocate within the cylinder. F_{SSy} is the lateral component of F_{SS}. The friction force of the slipper F_{FS} is generated as the slipper slides on the swash plate. The resultant force of F_{SSy} and F_{FS} is F_{L}. F_{FC} is the friction force between the cylinder and the piston, F_{C} is the centrifugal force of the piston, F_{I} is the inertial force of the piston, and F_{G} is the gravitational force of the piston. Due to the significant lateral force F_{L}, the piston tilts within the cylinder bore. This radial motion leads to a wedge-shaped oil film being squeezed. When the oil film becomes very thin, solid contact pressure arises. The resulting reaction force that balances the external forces is generated through a combination of the oil film's squeezing effect, dynamic pressure buildup, and solid contact pressure.

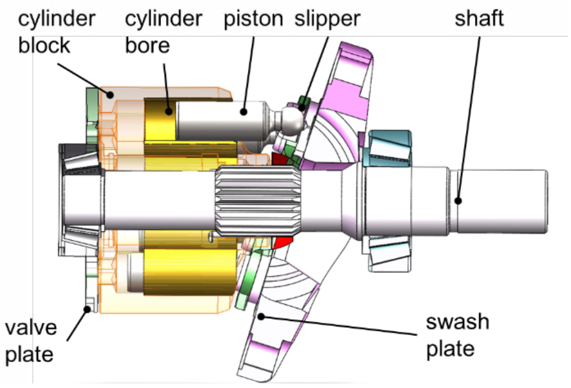

Figure 2.1. Axial piston pump basic structure

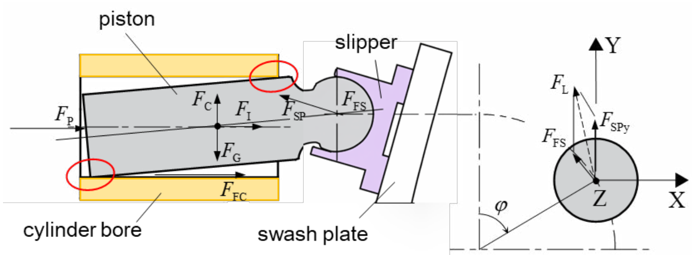

Figure 2.2. PCI dynamic analysis

The oil film thickness between the PCI is related to the posture of the piston in the cylinder bore. When the surface wear occurs, the wear depth $w(l,\theta)$ must be considered to achieve more accurate oil film thickness. Figure 2.3 shows the titling state of the piston in the cylinder bore exaggeratedly. The posture of the piston can be represented by the eccentricities of two sections relative to the cylinder bore. The oil film thickness can be defined as the clearance between the piston and the cylinder bore in the radial direction, and it is given by:

$$h(l,\theta) = (D_C - D_P)/2 + w(l,\theta) - [e_1 - (e_1 - e_2)l/L_C]cos\theta - [e_3 - (e_3 - e_4)l/L_C]sin\theta \quad (2.1)$$

where e_1, e_2 and e_3, e_4 are the eccentricities in the X direction and Y direction of the two sections respectively. L_C is the length of the cylinder bore, D_C and D_P are the diameter of the cylinder bore and the piston. The pressure field is divided into $a \times c$ grids and can be expanded to a plane for intuitive as shown in Figure 2.3.

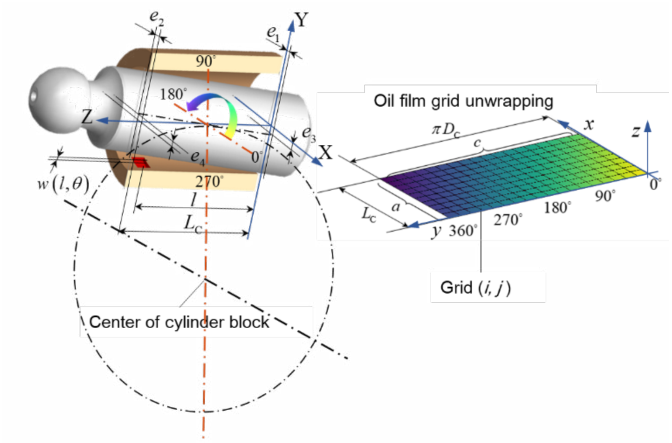

Figure 2.3. Titling state of the piston and expansion of the oil film

The minimum contact oil film thickness hm can be determined by the surface roughness of the friction pair is set to estimate whether the contact occurs. The definition of $h_{\min}$ [19] is shown in Eq. (2.1), where R_{qp} and R_{qc} are the root mean square roughness of the piston and the cylinder bore respectively:

$$h_{\min} = 3\sqrt{{R_{\mathrm{qp}}}^2 + {R_{\mathrm{qc}}}^2} \tag{2.2}$$

The hydrodynamic pressure of the oil film p can be represented by using Reynolds equation:

$$\frac{\partial}{\partial x}\left(\frac{\partial p}{\partial x}\frac{h^3}{\mu}\right) + \frac{\partial}{\partial z}\left(\frac{\partial p}{\partial z}\frac{h^3}{\mu}\right) = 6\left(\omega_{\mathrm{P}}\frac{D_{\mathrm{C}}}{2}\frac{\partial h}{\partial x} + u\frac{\partial h}{\partial z} + 2\frac{\partial h}{\partial t}\right) \tag{2.3}$$

where μ denotes the oil viscosity, and ω_{P} is the spinning speed of piston, u is the sliding velocity of the piston surface. To ensure numerical stability, the oil film thickness h is set to $h_{\min}$ when the calculated result of Eq. (2.2) is less than $h_{\min}$. In Eq. (2.3), the first two terms on the right-hand side represent the dynamic pressure effect generated by the wedge-shaped oil film, while the third term corresponds to the squeezing effect due to micro-scale radial motion of the piston. The Reynolds equation is discretized using the finite volume method, and the Cyclic Tridiagonal Matrix Algorithm is employed to solve the resulting pressure field of the PCI.

The pressure distribution is obtained by solving the discretized Reynolds equation, thereby determining the oil film reaction force acting on the piston. The Newton-Raphson method is then applied to iteratively solve the piston force balance equation.

In Figure 2.4, k is the rotated angle of the cylinder with the resolution of 1°. $\Delta\dot{e}$ is the variation of Δe in each iteration, adjusted automatically via the Newton-Raphson method. P, P_{cs} refers to dynamic oil film pressure and contact pressure between piston and cylinder block. F_{out}, F_{out}, F_{cs} refers to external force, dynamic oil film force and contact force between piston and cylinder block. A convergence threshold $F_{\mathrm{b}} = 0.1\ \mathrm{N}$ is set for the force balance residual. The Newton-Raphson iteration terminates when the condition $\|f(\dot{e}_k)\| \leq F_{\mathrm{b}}$ is satisfied. The simulation is considered converged and lubrication parameters are output when periodic phenomenon is exhibited.

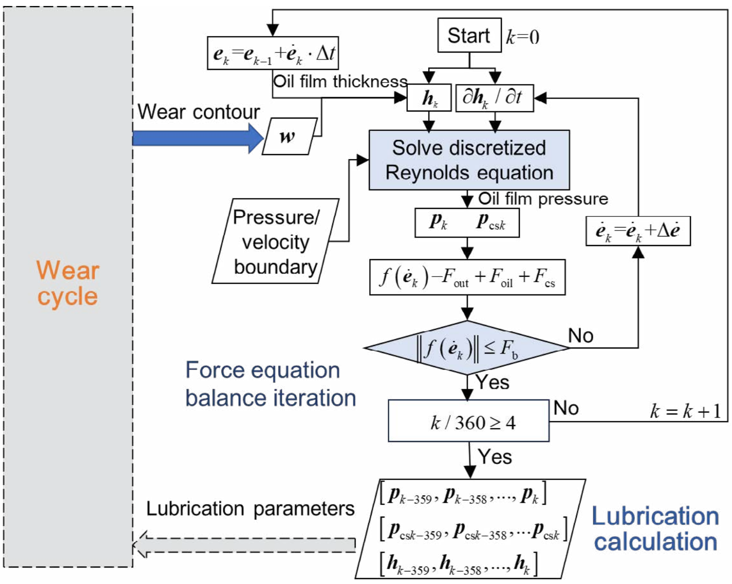

Figure 2.4. Schematic diagram of lubrication calculation

2.2. *Wear Cycle*

As shown in Fig. 2.5, inputs including the oil film thickness $h(i,j)$, pressure $p(i,j)$, and solid contact pressure $p_{cs}(i,j)$ field for each grid cell from the lubrication calculation model, as well as the contaminant particles size distribution d_{a} measured in the contaminated oil, are introduced into the wear cycle model. Depending on the local oil film thickness boundaries, each computational grid may undergo different wear mechanisms-including adhesive wear, two-body wear, and three-body abrasive wear-leading to distinct wear depths. And the wear contour is linearly superimposed with the revolutions until the wear depth exceeds a threshold value. Once the threshold is exceeded, the wear curve is fed into the oil film model to update the contours of both the piston and cylinder. The updated wear curve is also output, and the corresponding operating time can be calculated from the pump revolutions and speed. This completes the simulation of the time-varying wear process of PCI.

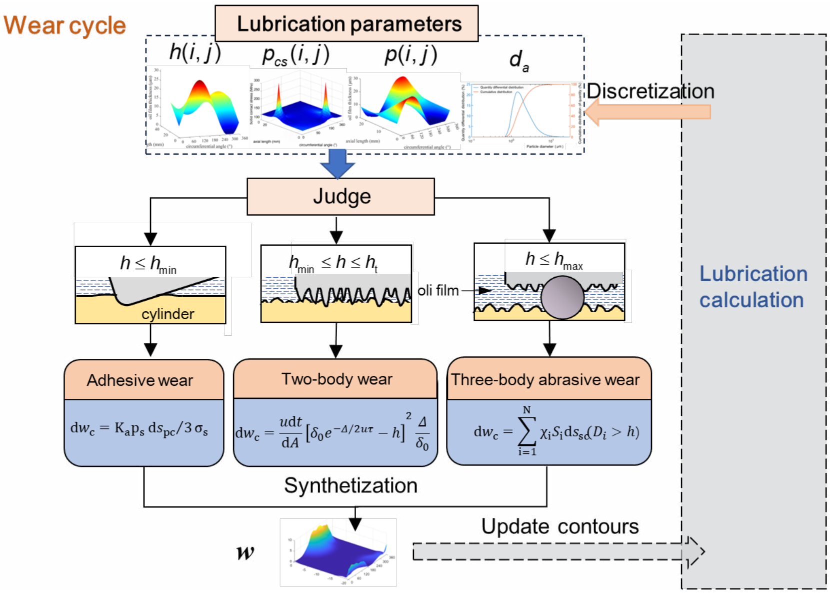

Figure 2.5. Wear cycle model

When the oil film cannot provide sufficient counterforce to balance the external load, the piston and cylinder are squeezed to slide against each other. Under high solid contact pressure, rupture of the oil film occurs, resulting in adhesive wear. The wear depth of the cylinder bore can be calculated using the equation below.

$$\begin{cases} 0 < h < h_{\min} \\ \mathrm{d}w = K_{\mathrm{a}} p_{\mathrm{s}} d_{\mathrm{pc}} / 3\sigma_{\mathrm{S}} \end{cases} \tag{2.4}$$

where d_{pc} is the displacement of the piston relative to the cylinder, σ_{S} is the compressive yield limit, K_{a} is the wear coefficient, p_{s} is the solid contact pressure.

When the oil film thickness is less than h_{t} which characterizes the height of the roughness peak after viscoelastic deformation but remains comparatively larger than the critical thickness $h_{\min}$ for adhesive wear, two-body wear may initiate. Specifically, two-body wear occurs when the deformed roughness peak exceeds the oil film thickness. The wear depth of the cylinder bore is shown below [27].

$$\begin{cases} h_{\min} < h < h_{\mathrm{t}} = \delta_0 \mathrm{e}^{-\Delta/2u\tau} \\ \mathrm{d}w_{\mathrm{c}} = \frac{u\mathrm{d}t}{\mathrm{d}A}\left[\delta_0 \mathrm{e}^{-\frac{\Delta}{2u\tau}} - h\right]\frac{\Delta}{\delta_0} \end{cases} \tag{2.5}$$

where t is the sliding time, and A is the wear area which is equal to the grid area of oil film thickness field, δ_0 is the height of roughness peak, Δ is the wavelength of roughness peak, τ is the delay time of the piston material.

As shown in the Figure 2.6, the real-time oil film contour formed by the reciprocating motion of the piston in the cylinder (as described in Section 2.1) exhibits a wedge-shaped oil film. The contamination level is used to determine the volume concentration within a particle size range. Laser analysis of the contaminated oil sample reveals the proportion of specific particle sizes, yielding the size and concentration distribution of the abrasive particles. When the particle size is smaller than the maximum oil film thickness, there is a certain probability χ_i that the particle will enter the PCI and cause wear [20]. Because the fluid is considered a homogeneous suspension, the probability of a particle entering the interface is assumed to be proportional to the volume of oil in the gap and the volume concentration of particles of different sizes. The influence of abrasive particles on adhesive wear extension is neglected in the simulation [21]. Wear primarily occurs in areas where the particle diameter exceeds the local oil film thickness, resulting in indentation and material removal [22]. In areas where the particle diameter is smaller than the oil film thickness, almost no wear occurs.

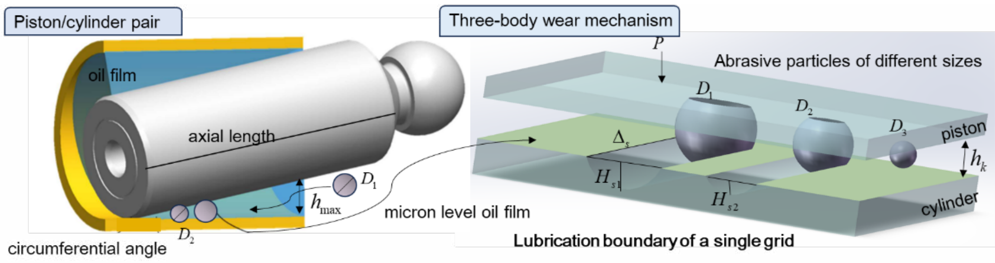

Figure 2.6. PCI three-body wear mechanism

Assuming the abrasive particles are spherical, for each simulation grid cell, particles of different sizes embedded into the cylinder surface will induce wear depths such as H_{S2} [23], which are inversely proportional to the hardness of both the cylinder and piston surfaces. When the particle diameter $D_i > h$, the wear depth on the cylinder can be calculated using Eq. (2.6). Since the size of the computational grid cell is much larger than the abrasive particle diameter, particles of different diameters $(D_1, D_2, \cdots)$ will cause wear in grid cells where the oil film thickness is less than the particle diameter. The cumulative wear volume per unit two-body distance is computed by summing the contributions from particles of various diameters. However, the displacement caused by abrasive particles on the cylinder surface is different from adhesive wear. According to the empirical formula that surface friction is inversely proportional to hardness [24], the sliding distance d_{sc} of the abrasive particles relative to the cylinder surface is calculated by torque balance and rolling kinematics, as shown in Eq. (2.7) and Figure 2.6(b). It is worth noting that different test conditions can produce two-body grooving or three-body rolling abrasive wear mechanisms [25]. For high-hardness abrasives such as quartz sand, when $D/h > 2$, particles may be embedded in the softer cylinder surface [26]. The sliding distance of the embedded particles relative to the piston surface becomes d_{pc}, which significantly increases wear and causes severe directional grooving on the harder surface. However, in this study, stainless steel powder with a hardness comparable to that of the cylinder material was used. The possibility of these particles adhering to the cylinder surface and causing scratches is very low.

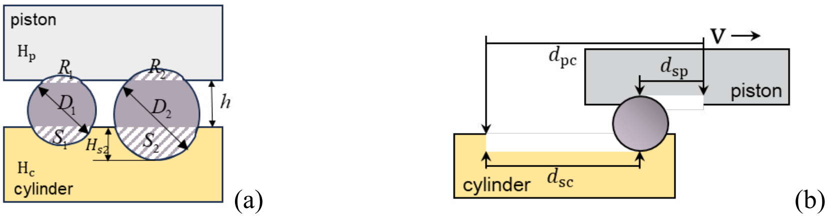

Figure 2.7. Three-body abrasive model

$$H_{\mathrm{S2}} = \frac{\mathrm{H_p}}{\mathrm{H_p}+\mathrm{H_c}}(D_i - h) \tag{2.6}$$

$$d_{\mathrm{sc}} = \frac{\mathrm{H_p}}{\mathrm{H_p}+\mathrm{H_c}} d_{\mathrm{pc}} \tag{2.7}$$

Where $\mathrm{H_C}$ and $\mathrm{H_P}$ are the hardness of the cylinder and piston, d_{pc}, d_{sc} and d_{sp} are the sliding distance relatively in Figure 2.7(b).

The wear volume of the cylinder and piston surface meshes is calculated by Eq. (2.8). Given that the calculated three-body wear volume of the piston is approximately 20% of the cylinder's and considering the piston's spinning motion (which promotes uniform axial wear distribution), the experimental analysis does not focus on the piston's wear contour. To optimize wear calculations, the wear contour is linearly superimposed with the revolutions until the wear depth exceeds a threshold value. Once the threshold is exceeded, the wear curve is fed into the oil film model to update the contours of both the piston and cylinder. The updated wear curve is also output, and the corresponding operating time can be calculated from the pump revolutions and speed. This completes the simulation of the time-varying wear process of PCI.

$$\begin{cases} \mathrm{d}w_{\mathrm{c}} = \sum_{i=1}^{\mathrm{N}} \chi_i S_i d s_{\mathrm{sc}} (D_i > h) \\ \mathrm{d}w_{\mathrm{p}} = \sum_{i=1}^{\mathrm{N}} \chi_i R_i d s_{\mathrm{sp}} (D_i > h) \end{cases} \tag{2.8}$$

Where $\mathrm{d}w_{\mathrm{c}}$ and $\mathrm{d}w_{\mathrm{p}}$ are the displacement of the abrasive particles relative to the cylinder and piston. χ_i is the probability of different abrasive particles participating in wear in this grid. S_i and R_i are the areas of the semicircular wear regions in Figure 2.7(a). D_i represents the set of abrasive particle diameters that can cause wear on the grid (i, j) with oil film thickness h.

3. EXPERIMENTAL INVESTIGATION

The isolated PCI test bench that can control the contamination level is designed to carry out the control test under NAS1638 8 and 12. The following is the detailed test method.

3.1. Test Bench Design

To experimentally validate the three-body abrasive wear simulation results of PCI across varying contamination levels, an isolated PCI test bench was built, capable of precisely and directly controlling the contamination levels in the PCI and isolating it from the influence of other friction pairs. In Figure 3.1, add external contamination and detect the contamination level of PCI through an online particle counter (9). Then switch the filter (2,12) through the directional valve (1,13) to control contamination level, when the contamination level gradually increases and exceeds the rated value during operation. The overflow valve (6) maintains the high-pressure input of PCI, and the driving swash plate speed is controlled by the driver (17). Actual picture of the isolated PCI test bench is shown in Figure 3.2.

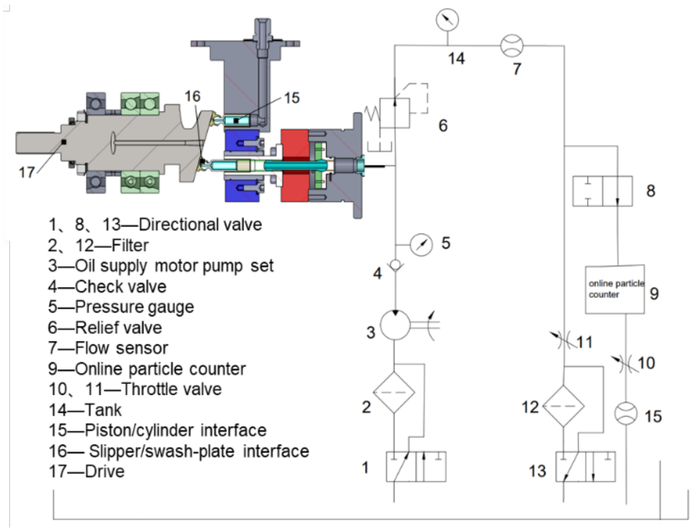

Figure 3.1. Hydraulic schematic diagram of the isolated PCI test bench

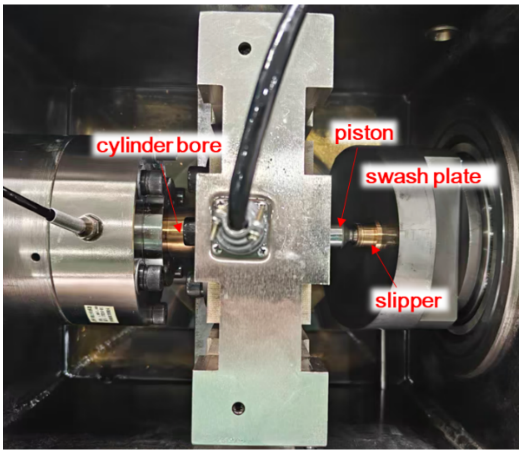

Figure 3.2. Physical photo of the isolated PCI test bench

3.2. Test Samples and Abrasive Particles Preparation

In Figure 3.3, the piston sample (a) and cylinder sample (b) used in this test are made of 38CrMoAl and manganese brass (CuZn37Mn3Al2PbSi) respectively, with a surface roughness of Ra 0.2μm after processing. The red mark is the effective length in contact with the piston.


(a)

(b)

Figure 3.3. Test samples

During the test run, 300 mL of oil with additional contaminated abrasive particles was taken, which was the same oil as that used in the PCI operating environment. The abrasive particles added to the oil are mixed with a mass ratio of 30% for <3 μm, 40% for 5 μm, and 30% for 6.5 μm to be closer to the actual contaminated oil abrasive particle distribution. An ultrasonic crusher was employed to ensure optimal dispersion of the particles. Subsequently, the contaminated oil sample underwent wet particle size analysis utilizing a laser particle sizer (Model LS-609, Zhuhai OMEC Instruments Co., Ltd., China). The particle size distribution measurement results are shown in Figure 3.4, and the proportion of each particle size can be obtained. Based on the aforementioned data, the differential percentage by count for specific particle size ranges (e.g., 5-15 μm, corresponding to the first interval of contamination level) can be further derived, as shown in Figure 3.5. Thus, based on the concentration of wear particles within the measured interval range (5-15 μm) detected by the contamination sensor, the proportion of each particle size required to participate in the wear cycle (Figure 2.5) is obtained, and the range is 0-30 μm.

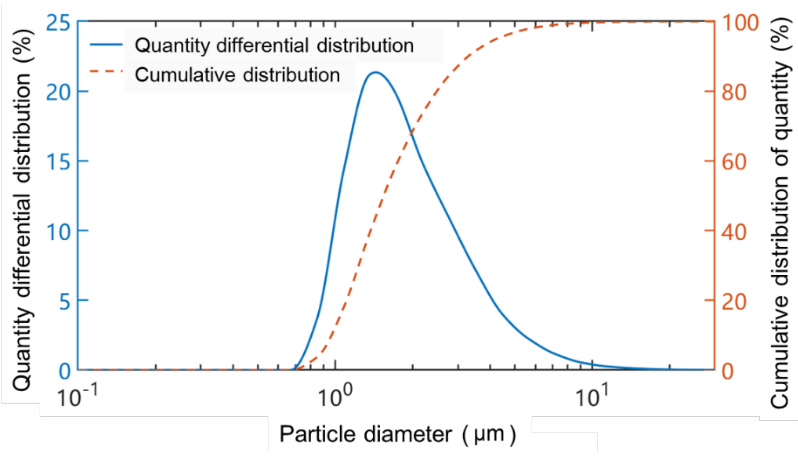

Figure 3.4. Particle size distribution

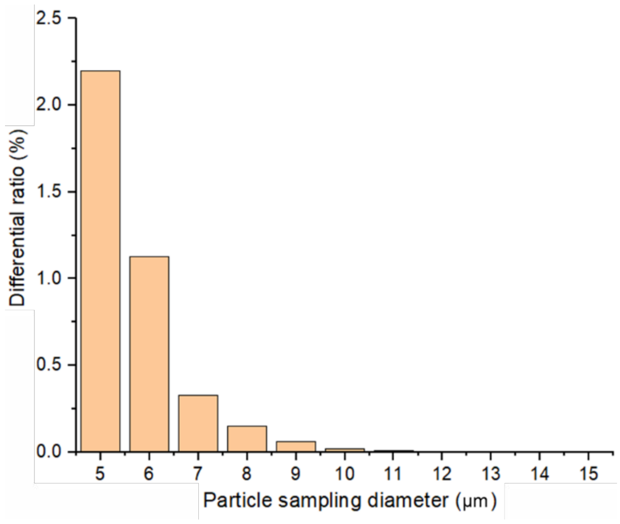

Figure 3.5. Different proportions of sampled abrasive particles

3.3. Experimental Procedures

The operating conditions were maintained at a pressure of 14 MPa and a rotational speed of 1500 rpm. A predetermined concentration of ultrasonically dispersed stainless steel contaminant particles was introduced into the 50 L oil tank. The oil supply motor pump was subsequently activated. After the hydraulic circuit and piston chamber were fully primed with oil, the system pressure was elevated to 14 MPa, corresponding to the preset cracking pressure of the relief valve. A minor volume of excess oil was discharged through a particle counter sensor integrated at the relief valve. Contaminant particles were supplemented in real time based on continuous monitoring until the oil contamination level stabilized. The drive motor was then engaged, and the rotational speed was increased to 1500 rpm to initiate the test. Whenever the contamination level exceeded the predetermined threshold, diversion filtration was activated to prevent particulate accumulation and clogging. Upon completion of the test, a recirculating filtration process was carried out for system flushing and cleaning.

The test was divided into two groups: one with clean oil without added particles, and the other with contaminated oil with a contamination level of 12, containing stainless steel abrasive particles. The two groups were run for 0.5 hours, 1.5 hours, 3 hours, and 5.5 hours, respectively. Stop at the set time, remove the sample and measure the inside of the cylinder using a three-coordinate instrument (Leitz PMM-C). The wear amount is calculated by subtracting the fitted contour before and after wear, thereby obtaining the wear process curve and contour change.

By monitoring the oil contamination level in real time with a particle counter sensor, the curve of the change in the number and volume of abrasive particles (5-15 μm) in the test with abrasive particles is shown in Fig. 14. It can be seen that the contamination level fluctuates within the range of 12. The small fluctuations observed in the experiment indicate the stability and reliability of the contamination control.

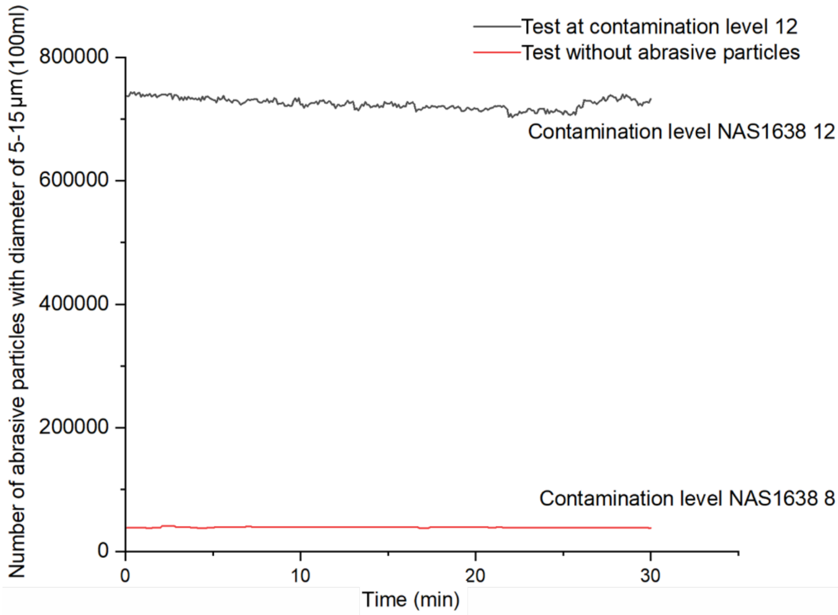

Figure 3.6 Fluctuations in contamination levels during the test

4. Results and Analysis

Figures 4.2(a) and (b) present the simulated wear contours of the cylinder surface with and without three-body abrasive wear, respectively. The three-body wear model in Figure 4.2(a) reveals a wear distribution extending 90°-360° around the cylinder port, with a depth of 0-7μm. Notably, severe wear is concentrated between 180° and 300° near the port. Additionally, moderate wear extends across the cylinder bottom from 0°-180° and 240°-360°. In contrast, the model without three-body wear in Figure 4.2(b) exhibits a significantly reduced wear zone, confined to 135°-340° at the port with a depth of 0-2.5μm and a distinct wear peak. The area of severe wear is limited, with only minor wear observed at the cylinder bottom.

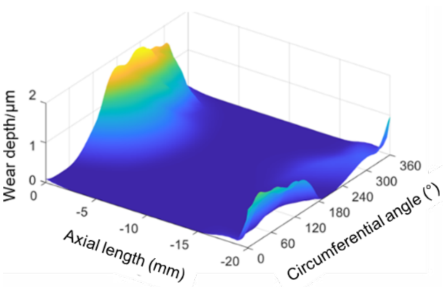

(a) with three-body abrasive wear

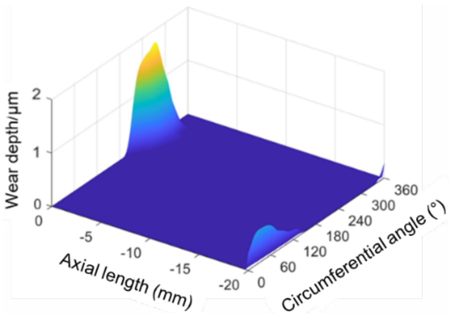

(b) without three-body abrasive wear

Figure 4.2. Simulated wear contour of the cylinder surface

Figure 4.4 shows the contour of cylinder after wear test at contamination level 12, while Figure 4.3 shows the contour of cylinder after wear without added abrasive particles. The wear contour is calculated by subtracting the run time after 0.5 hours from the wear time after 5.5 hours.

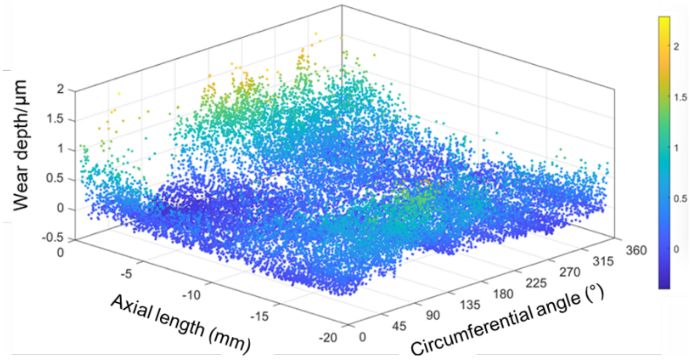

Figure 4.3. Contour of cylinder after wear test at contamination level 12

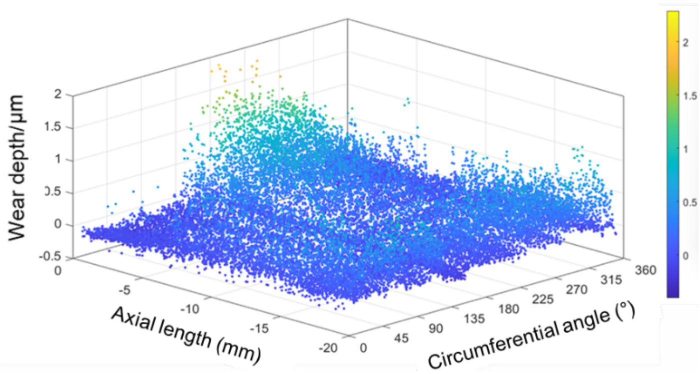

Figure 4.4. Contour of cylinder after wear without abrasive particles

Comparing the simulation results above, Figure 4.3 shows a similar wear range distribution to (a), with wear distribution at 90°-360° and 0-7μm in the cylinder port area, a larger wear distribution at 135°-290°, and a corresponding wear distribution at the bottom of the cylinder, only within a reasonable range of deviation. However, it is somewhat different from Figure 4.2(b), indicating that when the contamination level is high, the model including three-body wear is more accurate for simulation and has a more reasonable wear range.

Figure 4.4 shows the wear contour under the condition of no contamination. The distribution range of the larger wear is smaller, and the wear distribution is similar to the results of the model without the three-body abrasive particle addition, indicating that the wear process can be simulated without the three-body wear model under the condition of no contamination.

5. Conclusion

This paper introduces a predictive method for PCI wear that includes three-body abrasive wear due to oil contamination. Comparisons between simulated and experimental surface contours after operation under normal and highly contaminated (NAS1638 12) conditions reveal that, although the maximum wear depth is not significantly affected in the initial hours, the severe wear area and the overall worn area are greatly expanded. This accelerated wear process can deteriorate lubrication, potentially leading to premature failure. The model demonstrates a superior ability to predict both the wear extent and volume under high contamination, highlighting its significance for studying tribo-pairs in contaminated environments.

6. References

[1] Lyu, F., Zhang, J., et al. Research on wear prediction of piston/cylinder pair in axial piston pumps. *Wear*, 2020, 456-457: 203338.

[2] Zhang, J., Lyu, F., et al. Simulation and experimental investigation on low wear rate surface contour of piston/cylinder pair in an axial piston pump. *Tribology International*, 2021, 162: 107127.

[3] Yu, L., Wang, H., et al. A novel wear prediction method and wear characteristic analysis of piston/cylinder pair in axial piston pump. Wear, 2024, 550-551, 205402.

[4] Brinkschulte, L., Mutter, J., et al. An approach to wear simulation of hydrostatic drives to improve the availability of mobile machines [Paper presentation]. 11th International Fluid Power Conference (11. IFK), Aachen, Germany, 2018.

[5] Ivantysyn, R., Shorbagy, A., et al. Investigation of the wear behavior of the slipper in an axial piston pump by means of simulation and measurement [Paper presentation]. 12th International Fluid Power Conference (12. IFK), Dresden, Germany, 2020.

[6] Du, Z., Zhang, Y., et al. Research on Prediction Methods for Eccentric Wear of the Slipper Pair in Axial Piston Pumps and Lubrication Performance Analysis. *ASME Journal of Tribology*, 2024, 146(9), 092201.

[7] Horn, S., Ivantysyn, R., et al. Tribological properties of different slipper designs of an axial piston pump [Paper presentation]. 14th International Fluid Power Conference (14. IFK), Germany, 2024.

[8] Li, X., Zhang, J., et al. Multi-scale topography wear mechanism of the valve plate in axial piston pumps during running-in process: A case study. Engineering Failure Analysis, Volume 182, Part B, 110058, 2025.

[9] Aerospace Industries of America. *NAS 1638: Cleanliness Requirements of Parts Used in Hydraulic Systems*. Washington D.C., USA, 2001.

[10] Han, L., Zhao, X. An abrasive wear model between valve plate and cylinder block in axial piston pumps. Book Chapter CSAA/IET International Conference on Aircraft Utility Systems, 2018.

[11] Junhui Zhang, Yining Shen, et al. Tolerance design guideline for piston/cylinder interface of electro-hydrostatic actuator (EHA) pumps based on a Thermal-Fluid-Structure model. Tribology International, 2024, 191, 109208.

[12] Woldman, M. An experimental and theoretical investigation into three-body abrasive wear [PhD Thesis]. University of Twente, 2014.

[13] Koulocheris, D., Stathis, A., et al. Experimental study of the impact of grease particle contaminants on wear and fatigue life of ball bearings. *Engineering Failure Analysis*, 2014, 39: 164-180.

[14] Litwin, W., Kropp, S. Sliding bearings with sintered bronze bush lubricated by contaminated water with solid particles: Theoretical and experimental studies. *Wear*, 2023, 532-533: 205070.

[15] Zhao, X., Zhang, Y. Analysis of the tribological and dynamic performance of textured bearings under contaminated conditions. *Tribology International*, 2023, 187: 108732.

[16] Novak, N., Trajkovski, A., et al. Wear of hydraulic pump with real particles and medium test dust. *Wear*, 2023, 532-533: 205101.

[17] Qi, J., Liu, H., et al. Influences of added sand-dust particles on the tribological performance of graphite-like coating under solid-liquid lubrication. *Tribology International*, 2014, 71: 69-81.

[18] Qi, J., Wang, L., et al. The tribological performance of DLC-based coating under the solid-liquid lubrication system with sand-dust particles. *Wear*, 2013, 297(1-2): 972-985.

[19] Wen, S., Huang, P. *Principles of Tribology*. Wiley Online Library, 2012.

[20] Wang, L., Zhou, X., et al. Effect of sediment particle size on the friction and wear performance of NBR/copper rings under contaminated water lubrication conditions. *Wear*, 2025, 571: 205832.

[21] Baydoun S, Arnaud P, et al. Modelling adhesive wear extension in fretting interfaces: an advection-dispersion-reaction contact oxygenation approach. *Tribology International*, 2020, 151: 106490.

[22] Kusano, Y., Hutchings, I.M., et al. Modelling the entrainment and motion of particles in a gap: Application to abrasive wear. *Proceedings of the Institution of Mechanical Engineers, Part J: Journal of Engineering Tribology*, 2003, 217(6): 427-433.

[23] Adachi, K., Hutchings, I.M. Wear-mode mapping for the micro-scale abrasion test. *Wear*, 2003, 255(1-6): 23-29.

[24] Moore, A.J.W., Tegart, W.J.M. Relation between friction and hardness. *Proceedings of the Royal Society of London. Series A, Mathematical and Physical Sciences*, 1952, 212(1110): 452-458.

[25] Trezona, R.I., Allsopp, D.N., et al. Transitions between two-body and three-body abrasive wear: influence of test conditions in the microscale abrasive wear test. *Wear*, 1999, 225-229(Part 1): 205-214.

[26] Williams, J.A., Hyncica, A.M. Abrasive wear in lubricated contacts. *Journal of Physics D: Applied Physics*, 1992, 25(3A): A81-A90.

Biographies

Liangyu Song is a doctoral student in mechanical engineering hydraulics at Zhejiang University. His research interests focus on tribological analysis and predictive maintenance of hydrostatic pumps.

Fei Lyu received the Ph.D. degree in mechatronics engineering from Zhejiang University, Hangzhou, China, in 2022. He is currently a Post-Doctoral Researcher with the State Key Laboratory of Fluid Power and Mechatronic Systems, Zhejiang University and is conducting research exchanges at RWTH Aachen University in Germany. His research interests focus on tribological analysis and predictive maintenance of hydrostatic pumps and motors.

Junhui Zhang received the Ph.D. degree in mechatronics engineering from Zhejiang University, Hangzhou, China, in 2012.He is currently an Associate Professor with the State Key Laboratory of Fluid Power and Mechatronic Systems, Zhejiang University. He has authored or coauthored more than 60 articles indexed by SCI and applied for more than 30 National Invention Patents which are granted. He is supported by the National Science Fund for Excellent Young Scholars. His research interests include high-speed hydraulic pumps/motors and hydraulic robots.

Bing Xu received the Ph.D. degree in fluid power transmission and control from Zhejiang University, Hangzhou, China, in 2001. He is currently a Professor and a Doctoral Tutor with the Institute of Mechatronic Control Engineering and the Director of the State Key Laboratory of Fluid Power and Mechatronic Systems, Zhejiang University. He has authored or coauthored more than 200 journals and conference papers and authorized 49 patents. Dr. Xu is a Chair Professor of the Yangtze River Scholars Program and a Science and Technology Innovation Leader of the Ten Thousand Talent Program.